JACS Au
AN OPEN ACCESS JOURNAL OF THE AMERICAN CHEMICAL SOCIETY

pubs.acs.org/jacsau

Article

Polymer-Grafted Nanoparticles with Variable Grafting Densities for High Energy Density Polymeric Nanocomposite Dielectric Capacitors

Bhausaheb V. Tawade,*,⊥ Maninderjeet Singh,*,⊥ Ikeoluwa E. Apata, Jagadesh Veerasamy, Nihar Pradhan, Alamgir Karim,* Jack F. Douglas, and Dharmaraj Raghavan*

Cite This: *JACS Au* 2023, 3, 1365−1375

Read Online

ACCESS | Metrics & More | Article Recommendations | Supporting Information

ABSTRACT: Designing high energy density dielectric capacitors for advanced energy storage systems needs nanocomposite-based dielectric materials, which can utilize the properties of both inorganic and polymeric materials. Polymer-grafted nanoparticle (PGNP)-based nanocomposites alleviate the problems of poor nanocomposite properties by providing synergistic control over nanoparticle and polymer properties. Here, we synthesize "core−shell" barium titanate−poly(methyl methacrylate) ($BaTiO_3$−PMMA) grafted PGNPs using surface-initiated atom transfer polymerization (SI-ATRP) with variable grafting densities of (0.303 to 0.929) chains/nm^2 and high molecular masses (97700 g/mL to 130000 g/mol) and observe that low grafted density and high molecular mass based PGNP show high permittivity, high dielectric strength, and hence higher energy densities (≈ 5.2 J/cm^3) as compared to the higher grafted density PGNPs, presumably due to their "star-polymer"-like conformations with higher chain-end densities that are known to enhance breakdown. Nonetheless, these energy densities are an order of magnitude higher than their nanocomposite blend counterparts. We expect that these PGNPs can be readily used as commercial dielectric capacitors, and these findings can serve as guiding principles for developing tunable high energy density energy storage devices using PGNP systems.

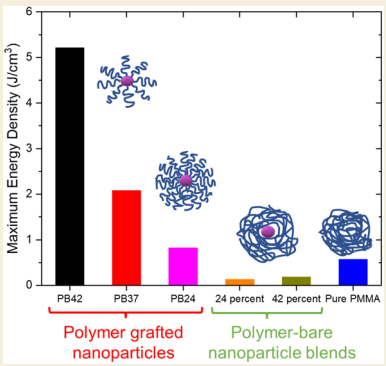

KEYWORDS: *$BaTiO_3$, PMMA, SI-ATRP, core−shell nanocomposites, polymer-grafted nanoparticles, dielectric constant, dielectric loss, energy storage, breakdown strength*

INTRODUCTION

The rising demand for high energy density and high power density devices necessitates innovation in energy storage processes and materials.[1] In particular, dielectric capacitors have the highest power density among energy storage devices. Dielectric materials can be classified into ceramic dielectrics and polymer dielectrics.[2−4] Among various ceramic-based dielectric materials, barium titanate ($BaTiO_3$) is of unique importance owing to its high dielectric constant (ε_r).[1,5,6] However, $BaTiO_3$-based dielectric materials typically have low dielectric strength and suffer from catastrophic failure, nonflexibility, etc.[1] On the other hand, polymeric dielectrics such as poly(methyl methacrylate) (PMMA) and polypropylene (PP) possess several advantages, including high dielectric breakdown strength, low dielectric loss, flexibility, formability, solvent processability, self-healing capability, and graceful breakdown failure over their inorganic counterparts.[1] Consequently, several research methods and strategies have been employed for developing energy storage systems based on polymer dielectrics.[1,7−10] The polymer-based dielectric materials normally have relatively low permittivities, resulting in lower energy densities than needed for advanced applications. As such, polymer nanocomposites containing ceramic nanoparticles and polymer matrices have been studied for achieving high permittivity as well as high dielectric strength. However, the nanocomposites in practice do not necessarily demonstrate the combined properties of the ceramic and polymers due to poor nanoparticle dispersion, agglomeration, field intensification at the nanoparticle−matrix interface, etc.[5,11]

Polymer-grafted nanoparticles (PGNPs), wherein polymers are grafted to nanoparticles, have emerged as good contenders for designing nanocomposites with highly dispersed nanoparticles, controlled nanoparticle spacing, and reduced property mismatch between the matrix and nanoparticle.[12,13] Bare nanoparticles, as in the case of hard spheres, do not pack very efficiently, and the presence of a "soft" grafted layer on the hard nanoparticle core allows for the grafted layer regions to overlap and deform.[14] This interpenetration of the grafted layers is also expected to lead to emergent elastic properties that should give the material elastic strength,[14] which is often found to correlate strongly with greater dielectric strength.[15−17] The reason for this general tendency of dielectric strength to increase with material strength is not

Received: January 10, 2023
Revised: April 11, 2023
Accepted: April 13, 2023
Published: April 26, 2023

well understood, but we may expect this trend to be beneficial in our development of dielectric strength of polymer materials based on PGNPs if the soft grafted polymer layer has appropriate properties giving rise to this type of rigidification phenomenon. Recent molecular simulation studies[17−19] have given some insight into the effect of the grafted layer on fluids of PGNPs where it is shown that a grafted layer of moderate grafting density can give rise to a strong reduction of the amplitude of density fluctuations in the material compared to linear polymers (a phenomenon termed "hyperuniformity"[17,19,20]) and the development of nontrivial collective motion and dynamic heterogeneity having a phenomenological similarity to glass-forming liquids.[18,21] Qualitative aspects of this enhanced packing found in PGNPs and related star polymers having a moderate number of arms have been illuminated in other recent studies.[15,16,22] We can then expect competing effects associated with the polymer grafting density, polymer chain length, chain flexibility, polymer nanoparticle interaction strength, and nanoparticle core size that should influence the capacity of the polymer-grafted nanoparticles to interpenetrate. It is evident, for example, if the grafting density of chains grown from the surface of the nanoparticles is very high so that the grafted layer becomes a relatively uniform density brush, then their packing must be rather like their hard cores so that the elastic stabilization and corresponding increase of the dielectric strength would be lost even though this limit should be good for achieving good nanoparticle dispersion. We must then expect trade-offs to be observed in the ultimate properties of these materials as these molecular parameters are varied, and we find below evidence that this is the case. With regard to the advance of polymer grafting as an approach for developing improved nanoparticle−polymer "blends", we note that another advantage is that processing of these materials does not require the addition of compatibilizer additives that can lead to the undesirable slow "aging" of the material properties associated with phase separation. Furthermore, the matrix-free PGNPs yield high loadings of nanoparticles while maintaining the favorable properties of nanoparticles as well as polymers, thus enabling high-performance nanocomposite materials.[23,24] The approach of using different molecular masses and grafting densities has been used to tune the gas permeability properties as well as mechanical properties in pioneering work by Kumar and co-workers.[25,26] Bockstaller and co-workers have demonstrated the effect of the grafting density and molecular mass on the mechanical properties of polymer-grafted nanoparticle-based films.[27]

In regards to the grafting feasibility, polymers can be facilely grafted onto titania (TiO_2) nanoparticles (NPs) as well as $BaTiO_3$ NPs using different methods such as the "grafting-to" method which involves the attachment of end-functionalized polymer chains on the surface of nanoparticles via suitable chemical reactions.[28] This involves nanoparticle surface modification by silylation, followed by click reactions including thiolene, epoxy−amine, etc. This method has been utilized for the grafting of polystyrene (PS), PMMA, and poly(vinylidene fluoride) (PVDF) to $BaTiO_3$ NPs.[29−31] The major disadvantage of the grafting-to method is the difficulty in achieving PGNPs having a high graft density due to the steric hindrance occurring in grafting-to reactions. Another approach is template-assisted synthesis, which involves the crystallization of $BaTiO_3$ nanoparticles within the specific area of the template. This method has been efficiently used for the fabrication of core−shell nanomaterials with precise control of structures and morphologies.[32−35] However, template-assisted synthesis has not been widely used because of the difficulty in scalability. Lastly, the "grafting-from" method involves the use of surface-initiated controlled radical polymerizations such as atom transfer radical polymerization (ATRP),[36−45] and reversible addition−fragmentation chain transfer (RAFT) polymerization[46,47,56,48−55] is another method to grow polymer chains directly from the surface of the nanoparticle. This approach has been used for the synthesis of well-defined polymer-grafted $BaTiO_3$ nanoparticles.

Structure−property relationship studies of polymer-grafted $BaTiO_3$ nanoparticle cast nanocomposites have demonstrated that several factors influence the dielectric performance of these nanocomposites, such as the radius of the nanoparticle core, the thickness of the grafted polymer layer of the core−shell nanoparticles, type of polymer grafted on the nanoparticles,[35,40] and separation between nanoparticles cores.[41] The type of interfacial layer can also be varied, and multiple polymers have been utilized to create a "double-shell" grafted layer around the solid nanoparticle cores.[44] Yang et al.[30] reported the utilization of thiol−ene click reaction for grafting PS or PMMA on $BaTiO_3$ nanoparticles surface to investigate the effect of molecular mass of polymer-grafted chains and graft density ($BaTiO_3$ NPs size: ≈100 nm; graft density = (0.072 to 0.585) chains/nm^2; molecular mass: 10K (graft density = 0.585 chains/nm^2) to 80K (graft density = 0.072 chains/nm^2); energy density: 0.02 J/cm^3 at 10 kV/mm) on the dielectric performance of nanocomposite. However, due to the limitation of the grafting-to approach, they were unable to synthesize high graft density PGNPs with high molecular mass polymer chains.

Here we report on the role and effect of low and high grafting density of high molecular mass polymers, grafted onto $BaTiO_3$ nanoparticles, on their dielectric performance in these one-component PGNP nanocomposite films, prepared by solution processing. The high molecular mass of the PMMA-grafted chains enable film casting with solution processing. We synthesized PMMA-grafted $BaTiO_3$ nanoparticles with high molecular mass and with different graft densities using the "grafting-from" method via SI-ATRP polymerization. The grafting density and molecular mass were tuned with varying the feed ratio of monomer to ATRP initiator functionalized $BaTiO_3$ NPs. The synthesized PMMA-grafted $BaTiO_3$ NPs provide unique strategies to disperse nanoparticles in polymer matrices by preventing aggregation while enhancing the desired properties of the polymer nanocomposites.[12] Furthermore, the PGNPs can be conveniently and relatively rapidly solution-processed into polymer nanocomposite films free from matrices, thereby producing polymer films with high nanoparticle loadings (up to ≈42 mass %). We observe that the low grafting density and high molecular mass based PGNPs show high permittivity, high dielectric strength, and hence high capacitive energy densities (≈5.2 J/cm^3), which are higher than those for higher grafted density PGNPs and an order of magnitude higher than their blend counterparts. We anticipate that the high dielectric strength of low grafted-density PGNPs is due to the overlap and entanglement of grafted polymers in these "soft shell" PGNPs. The grafting density effects demonstrated in this study are expected to influence the mechanical properties,[57] ionic conductivities,[58] and macroscopic superlattices[59] of PGNPs, in addition to the dielectric properties studies here.

https://doi.org/10.1021/jacsau.3c00022
JACS Au 2023, 3, 1365−1375

MATERIALS AND METHODS

Materials

$BaTiO_3$ nanoparticles (50 nm), 30% aqueous H_2O_2 solution, (3-aminopropyl)trimethoxysilane (APTMS), α-bromoisobutyryl bromide (BIB), triethylamine, methyl methacrylate (MMA), styrene, copper(I) bromide (CuBr), *N*,*N*,*N*′,*N*″,*N*‴-pentamethyldiethylenetriamine (PMDETA), 40% hydrofluoric acid (HF), *N*,*N*-dimethylformamide (DMF), toluene, tetrahydrofuran (THF), and dichloromethane (DCM) were purchased from Sigma-Aldrich Chemical Co. MMA and styrene were distilled under vacuum before use whereas all other reagents and solvents were used as received. The homopolymer PMMA used in this study was purchased from Polymer Source and had a molecular mass of 106000 g/mol.

Synthesis

Step I: Surface Hydroxylation of $BaTiO_3$ Nanoparticles by Treatment with H_2O_2. $BaTiO_3$ nanoparticles (5.11 g) and a 30 mass % aqueous H_2O_2 solution (30 mL) were placed in a 250 mL round-bottom flask. The reaction mixture was interchangeably stirred, sonicated for about 1 h, and then refluxed under nitrogen at 105 °C for 4 h. The modified nanoparticles were recovered upon centrifugation at 5000 rpm for 10 min and washed several times using deionized water. The recovered white powder of hydroxylated $BaTiO_3$ nanoparticles (BT-OH) was dried under vacuum at 80 °C until a constant mass.

Step II: Modification of $BaTiO_3$-OH (BT-OH) with APTMS. BT-OH (2 g) and toluene (10 mL) were placed in a 25 mL round-bottomed flask and interchangeably stirred and sonicated for 1 h. APTMS (1 g) was added to the mixture, and the reaction mixture was heated at 80 °C for 24 h under a nitrogen atmosphere. At the end of the 24 h, silylated $BaTiO_3$ NPs were recovered from the reaction mixture by centrifugation at 10000 rpm for 10 min followed by washing several times with toluene. The recovered APTMS-modified $BaTiO_3$ nanoparticles (BT-APTMS) were dried under vacuum at 80 °C for 12 h.

Step III: Modification with BIB (α-Bromoisobutyryl Bromide). APTMS-modified $BaTiO_3$ (1 g) nanoparticles (BT-APTMS) and 15 mL of DCM were placed in a 50 mL round-bottomed flask and interchangeably stirred and sonicated for 1 h. Trimethylamine (101 mg, 0.140 mL) was added to the solution, and CH_2Cl_2 solution containing 0.56 g of α-bromoisobutyryl bromide (229.9 mg, 124 μL) was then added in a dropwise manner and stirred at 0 °C for 1 h. The entire reaction mixture was stirred at 0 °C for 3 h followed by additional stirring at room temperature for 20 h. Subsequently, the nanoparticles were recovered by centrifugation at 5000 rpm for 10 min followed by washing several times with CH_2Cl_2. The obtained initiator-modified $BaTiO_3$ nanoparticles were dried under vacuum at 80 °C for 12 h. FT-IR and TGA were used to characterize the Br-APTMS-$BaTiO_3$ nanoparticles.

Step IV: SI-ATRP of MMA from $BaTiO_3$ (PB42). Br-APTMS-$BaTiO_3$ (0.050 g) and 5 mL of DMF were placed in a Schlenk flask and interchangeably stirred and sonicated for 1 h. 0.025 g of CuBr was added, and the flask was sealed with a rubber plug. The oxygen in the flask was carefully removed by evacuating and backfilling with N_2 gas three times. For example, to synthesize PB42 sample, MMA (2.5 g, 2.66 mL) and 0.030 g of PMDETA were added by syringe to the reaction flask, and a freeze−thaw pump cycle was performed three times to degas the reaction mixture. This reaction mixture was then stirred at 65 °C for 24 h. The product was then precipitated in acetone and recovered by centrifugation at 10000 rpm for 10 min. The polymer-grafted BT nanoparticles were washed several times in acetone to remove the ungrafted polymer from the PGNPs. The obtained PMMA-grafted $BaTiO_3$ (PMMA-*g*-$BaTiO_3$) nanoparticles were dried under vacuum at 80 °C for 12 h.

To obtain PMMA-*g*-$BaTiO_3$ nanoparticles with different graft densities and molecular mass, the polymer grafting experiment was performed by changing the feed ratio of $BaTiO_3$-APTMS-Br (2%, 5%, 7.5%) to the mass of MMA (while keeping the other parameters constant), and the resultant nanoparticles were labeled as PB42 (42 mass % $BaTiO_3$), PB37 (37 mass % $BaTiO_3$), and PB24 (24 mass % $BaTiO_3$).

Step V: Cleavage of Grafted Chains from the Polymer Grafted $BaTiO_3$ Nanoparticles. In a typical experiment, PMMA-*g*-$BaTiO_3$ (0.020 g) was placed in a Teflon flask, and 5 mL of THF was added. The mixture was dispersed via sonication for 30 min, then 0.5 mL of an aqueous solution of HF (40 mass %) was added, and the mixture was allowed to stay overnight with continuous stirring at room temperature. The cleaved sample was centrifuged to separate nanoparticles from polymer-grafted chains. The solution containing cleaved PMMA was concentrated and precipitated in hexane to obtain PMMA, which was further characterized by gel permeation chromatography (GPC) and nuclear magnetic resonance (NMR) analysis.

Characterizations

FT-IR Spectroscopy. FT-IR spectra of nanoparticles were collected using a PerkinElmer Spectrum 100 series ATR-FTIR spectrometer.

NMR Spectroscopy. ^{1}H NMR spectra of cleaved polymer samples were recorded on a Bruker AVANCE 400 ^{1}H NMR (400 MHz) spectrometer. Chemical shifts are given in parts per million (δ ppm) relative to tetramethylsilane (TMS). For ^{1}H NMR spectra, peaks are calibrated to 7.26 δ ppm.

Thermogravimetric Analysis (TGA). TGA of the $BaTiO_3$, surface-modified $BaTiO_3$, and PMMA grafted $BaTiO_3$ was conducted using a TGA/DTA 320 Seiko instrument under a nitrogen atmosphere (flow rate of 100 mL min^{-1}). The thermogram was generated by placing nearly 10 mg of samples in a pan and heating it from 30 to 600 °C at a heating rate of 10 °C min^{-1}.

Gel Permeation Chromatography (GPC). Molecular mass measurements of cleaved polymers were performed by GPC on an Agilent Technologies 1260 Infinity instrument. Polystyrene standards were used for calibration. THF was used as the eluent, and the typical sample concentration was 1 mg mL^{-1}.

Graft Density Calculations

The grafting density (σ_{TGA}) was calculated from the TGA analysis using eq 1. The relative mass of the polymer (mass % shell) grafted on the nanoparticles and the residual mass of the BT nanoparticle were extracted from the experimental TGA data at 600 °C[60]

$$\sigma_{TGA} = \frac{\frac{\text{wt \%}_{shell}}{\text{wt \%}_{core}} \rho_{core} \frac{4}{3}\pi r_{core}^{3} N_A}{M_w 4\pi r_{core}^{2}} \quad (1)$$

where mass % of shell = (char yield of the PGNPs) − (char yield of BT nanoparticle), mass % of core = char yield of BT nanoparticle, N_A = Avogadro's number, ρ_{core} = 6.09 g/cm^3, which represents the density of bulk $BaTiO_3$, r_{core} = 50 nm, which correspond to the radius of $BaTiO_3$ assuming its spherical shape, and M_w = mass average molecular mass of cleaved polymer chains.

Film Formation

The PMMA-*g*-$BaTiO_3$ NPs were dissolved in toluene in ratios of 2−10 mass %. The solutions were mixed on a vortex shaker for 24−48 h to ensure complete dispersion of the PMMA-*g*-$BaTiO_3$ in the solvent. The pristine PMMA homopolymer was dissolved in toluene to make solutions with concentrations ranging from 2 to 10 mass %. The $BaTiO_3$ nanoparticles were added to the polymer solutions in the mass ratios of 42, 37, and 24 mass % with respect to the polymer for comparison with PGNPs. The PMMA-*g*-$BaTiO_3$ solutions and the PMMA−$BaTiO_3$ nanoparticle blend solutions were drop-cast on aluminum-coated (≈100 nm using ultrahigh-vacuum sputtering) silicon substrates (purchased from University Wafers) to yield film thicknesses ranging from approximately 2 to 6 μm. The film thicknesses were measured using AFM scratch tests.

Dielectric Breakdown and Permittivity Testing

The dielectric breakdown testing was performed using the PolyK system PK CPE-1801. The polymer-grafted nanoparticle (PMMA-*g*-$BaTiO_3$), pristine polymer (PMMA), and polymer−nanoparticle

https://doi.org/10.1021/jacsau.3c00022
JACS Au 2023, 3, 1365−1375

Table 1. Results of SI-ATRP Polymerization of MMA from the $BaTiO_3$ Surface

sample name	particle to monomer ratio (mass %)	MMA:BT-APTMS-Br:CuBr(I)	M_n[a] (g/mol)	M_w (g/mol)	dispersity	shell thickness[b] (nm)	BT content in PGNPs (mass %) (from TGA)
PB42	2	50:1:0.5	101900	130000	1.27	5−9	42.7
PB37	5	20:1:0.5	71200	100000	1.40	5−8	37.4
PB24	7.5	13.33:1:0.5	53600	97700	1.82	≈7	24.1

[a]Molecular masses were obtained from GPC of polymer cleaved PMMA-*g*-$BaTiO_3$ samples. [b]Shell thickness range—calculated from image analysis of multiple TEM micrographs.

Scheme 1. Synthesis of PMMA-*g*-$BaTiO_3$ (PB) Nanoparticles

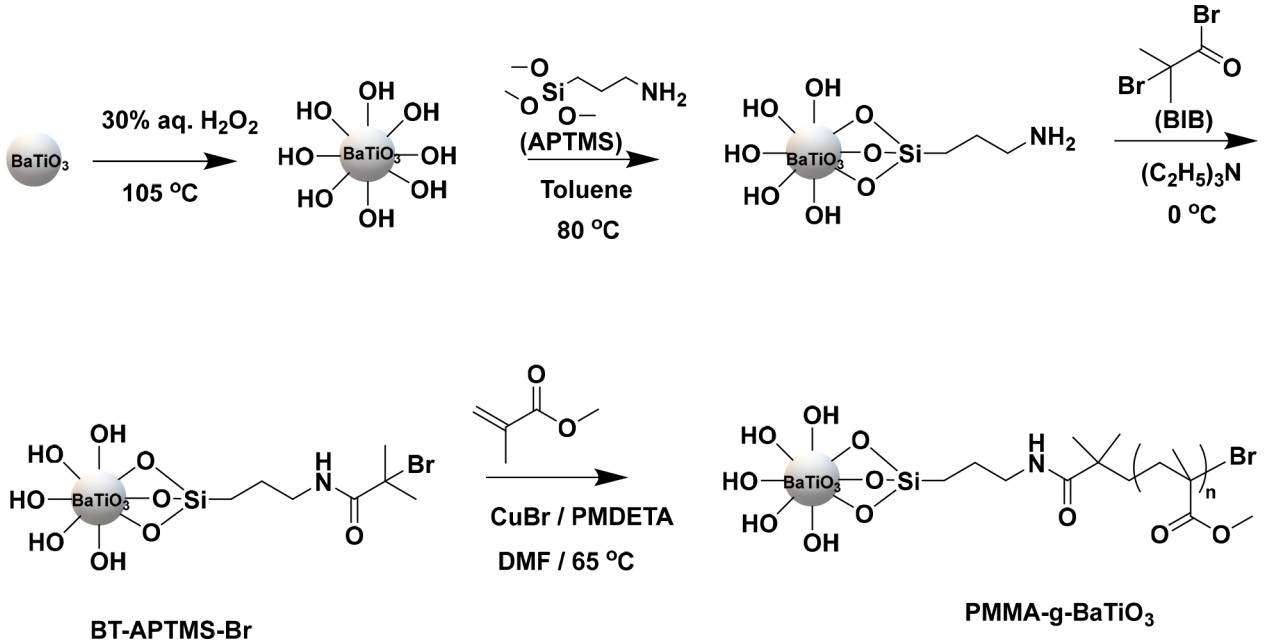

blend (PMMA−$BaTiO_3$) films on the conductive substrate were contacted with spring-loaded electrodes to generate point contacts. The DC electric field was applied on the films with a ramp rate of 20 V/s, and the breakdown values were recorded using the PolyK software. The breakdown occurs when ≈1 mA of current passes through the films. Typically, ≈15 breakdown points were measured per film, and the data was analyzed using Weibull failure analysis, i.e., $P(E) = 1 - \exp[-(E/E_{BD})^{\beta}]$, where $P(E)$ is the probability of failure, E is the measured dielectric strength, and E_{BD} is the Weibull dielectric strength, i.e., the dielectric strength at a failure probability of 63%. Here, β is a parameter that describes how much the shape of the relaxation function deviates from being exponential.

The permittivity and the loss tangent data were calculated using dielectric spectroscopy measurements with a Keysight E4980 AL LCR meter. The top electrodes on the polymer-grafted nanoparticle and polymer−nanoparticle blend films were fabricated using the eutectic gallium−indium liquid metal, and the data were recorded in the desired frequency range.

RESULTS AND DISCUSSION

Core−shell structured PMMA-*g*-$BaTiO_3$ NPs were synthesized by slightly modifying the reported literature[37] procedure of the "grafting from" approach. The different samples synthesized were labeled as PB42 (41.7 mass % $BaTiO_3$), PB37 (37.4 mass % $BaTiO_3$), and PB24 (24.08 mass % $BaTiO_3$) depending on their $BaTiO_3$ content, and the complete characteristics of these samples are highlighted in Table 1. The four-step procedure of synthesizing PMMA-*g*-$BaTiO_3$ NPs consists of hydroxylation with H_2O_2 followed by silylation (APTMS), anchoring of ATRP initiator (BIB) agent, and the final step of SI-ATRP polymerizations of MMA on $BaTiO_3$ nanoparticles. The stepwise route for the synthesis is depicted in Scheme 1. The FTIR spectra of surface-modified $BaTiO_3$ nanoparticles after every step is shown in Figure S1. First, the surface of the $BaTiO_3$ nanoparticles was activated by treatment with hydrogen peroxide. The decomposition of H_2O_2 on the surface of NPs generates hydroxyl groups on the $BaTiO_3$ nanoparticle's surface.[61] This is confirmed by the slight increase in the broadness of the −OH stretching peak around 3400−3600 cm^{-1} as observed in the FTIR spectra for the BT-OH (Figure S1), which could be attributed to the formation of a higher concentration of −OH groups on the surface of $BaTiO_3$ nanoparticle. Subsequently, the hydroxylated $BaTiO_3$ was subjected to a silylation reaction with APTMS which led to the anchoring of amino functionality on the nanoparticle surface. The anchoring of the APTMS was established by the appearance of alkyl stretching at 2900 cm^{-1} due to aliphatic −C−H in APTMS as observed in the FTIR spectra for BT-APTMS (Figure S1). The $BaTiO_3$-APTMS was further reacted with 2-bromoisobutyryl bromide (BIB) to synthesize initiator functionalized $BaTiO_3$ nanoparticle ($BaTiO_3$-APTMS-Br). The carbonyl stretching at 1650 cm^{-1} due to −CONH− (amide) groups was noticed in the spectra for BT-BIB indicative of BIB moiety attachment to the $BaTiO_3$ surface. Finally, SI-ATRP of MMA on $BaTiO_3$-APTMS-Br nanoparticles resulted in the surface functionalization of nanoparticles (PMMA-*g*-$BaTiO_3$) as evidenced by the appearance of the characteristic peak of −C═O at 1722 cm^{-1}.

https://doi.org/10.1021/jacsau.3c00022
JACS Au 2023, 3, 1365−1375

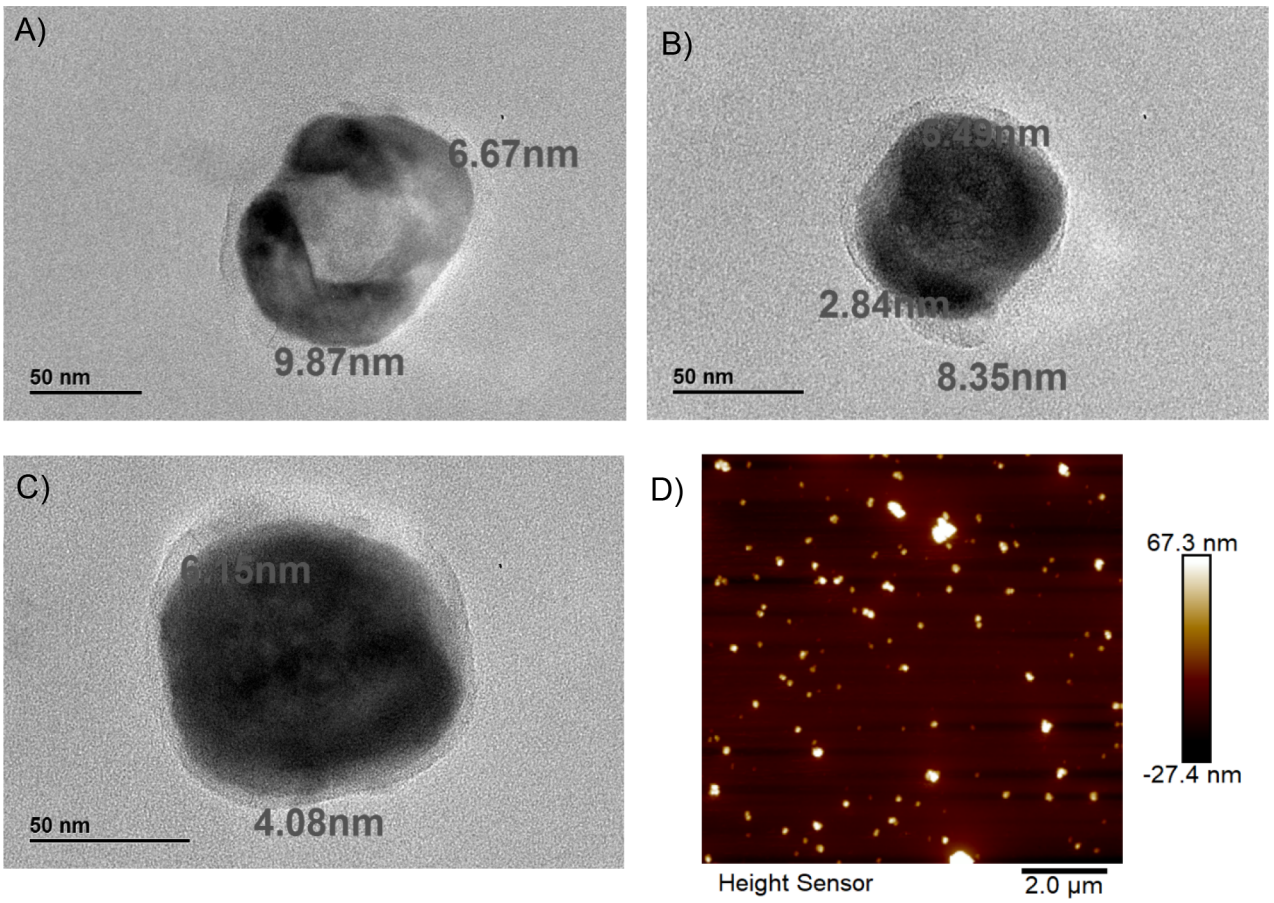

Figure 1. Transmission electron microscopy (TEM) images of PMMA-*g*-$BaTiO_3$: (A) PB42, (B) PB37, and (C) PB24. (D) Atomic force microscopy (AFM) image showing the dispersion of PMMA-*g*-$BaTiO_3$ PGNPs in single-component films.

Figure S2 depicts the ^{1}H NMR spectrum of the polymer cleaved from PMMA-*g*-$BaTiO_3$ NPs (PB24); the broad signal at 3.65 δ ppm corresponds to $-OCH_3$, multiplets in the range 0.84−1.21 δ ppm correspond to $-CH_3$, and the multiplets in the range 1.43−2.06 δ ppm correspond to $-CH_2-$ of the PMMA backbone. The characteristic peaks of the PMMA noticed in the ^{1}H nuclear magnetic resonance (NMR) spectrum of cleaved polymer strongly suggests that PMMA is indeed grafted onto $BaTiO_3$ nanoparticles.

The cleaved polymer samples were also characterized by gel permeation chromatography (GPC) measurements, and the results of GPC are presented in Table 1 (Figures S3−S6). The molecular masses of grafted polymer chains on $BaTiO_3$ nanoparticles were in the range of 97700−130000 g/mol and were found to be a function of the feed ratio of $BaTiO_3$ nanoparticles and MMA. The median value of polydispersity was close to 1.4, indicating good control in the molecular mass of polymer grafted on the nanoparticles using ATRP polymerization. Aside from the reasonable control in the polydispersity of molecular mass of the high molecular mass polymer grafted nanoparticles, we also varied the graft density of the polymer grafted nanoparticles by varying the feed ratio. For the MMA concentrations studied, the polymerization rates of polymer grafted on the nanoparticles were found to be dependent on the concentration of monomer used. A higher rate of polymerization is expected for systems where a high concentration of the monomer was used. Furthermore, the use of a high concentration of the monomer in the reaction mixture could influence the dispersibility of the nanoparticle in the reaction mixture. A high concentration of the monomer in the reaction mixture results in poor dispersion of initiator-grafted $BaTiO_3$ NPs in the reaction mixture, which leads to a decrease in the available sites on the nanoparticles (reduced surface area) for the polymerization. To support the explanation put forth, dynamic light scattering (DLS) analysis was conducted of initiator-grafted $BaTiO_3$ NPs in different mixtures of MMA and DMF. The initiator-grafted $BaTiO_3$ NPs exhibited excellent dispersion in the DMF (lowest *z*-average size) while poor dispersion (increase in *z*-average size) was noticed with an increase in the concentration of MMA in the reaction mixture (Figure S7). In addition, the variation in the monomer concentration with respect to $BaTiO_3$ NPs also resulted in the variation of concentration of the "CuBr(I)" catalyst leading to different graft densities.[62] A lower catalyst copper concentration for PB42 resulted in a lower graft density while a high concentration of PB24 resulted in a high graft density. Therefore, the variation rate of the polymerization reaction and the dispersion of initiator-grafted $BaTiO_3$ NPs at different loading compositions afforded formulation of high molecular masses and a range of $BaTiO_3$ PGNPs with varying graft density.

Transmission electron microscopy (TEM) was used to observe the morphology and dispersion of the synthesized PMMA-*g*-$BaTiO_3$ NPs in the solvent used for solution processing. Figure 1 presents TEM micrographs of cast PMMA-*g*-$BaTiO_3$ nanoparticles film. Clearly, in the TEM images, we observe a lighter corona coating layer which corresponds to the grafted polymer shell and a relatively darker

https://doi.org/10.1021/jacsau.3c00022
JACS Au 2023, 3, 1365−1375

shade core $BaTiO_3$ nanoparticle. Image analysis was used to calculate the shell thickness of the polymer layer. Table 1 presents the sample identity and respective thickness of the polymer shell. The shell thickness showed a slight increase as a function of the feed ratio of the monomer used for polymer grafting. Furthermore, we noticed the grafting of the PMMA on the $BaTiO_3$ surface also improved the dispersion of the nanoparticles in solution processable solvent. The morphology of drop-cast film of PMMA-*g*-$BaTiO_3$ NPs was also analyzed by atomic force microscopy (AFM). AFM also validated good dispersion of PMMA-*g*-$BaTiO_3$ NPs in solvent (Figure 1D), indicating grafted PMMA chains restrict agglomeration of $BaTiO_3$ NPs in a solution processable solvent.

Figure 2 shows the thermograms of bare NPs and PMMA-*g*-$BaTiO_3$ PGNPs. The char yield value derived from TGA measurement was used to estimate the amount of polymer grafted on the $BaTiO_3$ nanoparticles. The char yield of various PMMA-*g*-$BaTiO_3$ PGNPs was found to be varied with variation in the concentration of monomer polymerization reaction. PB42 yields a char value of 41.7 mass %, PB37 yields a char value of 37.4 mass %, and PB24 yields a char value of 24.08 mass % indicative of the extent of polymer grafted on the nanoparticles. A similar decrease in the char yield of the PMMA-*g*-$BaTiO_3$ NPs was observed when MMA was diluted with anisole.[38]

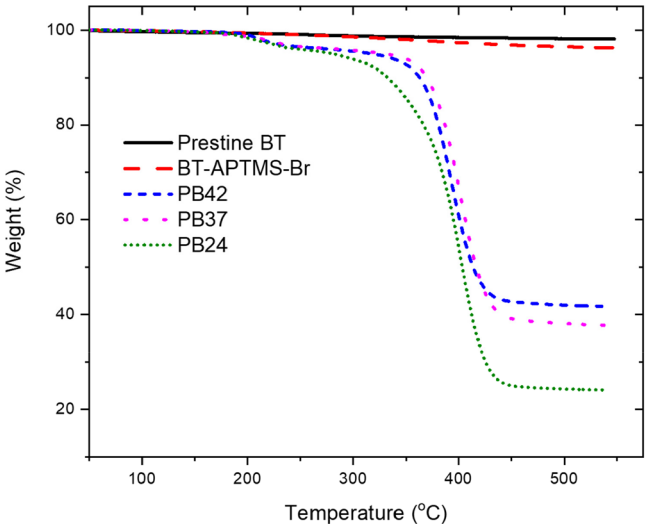

Figure 2. Thermogravimetric analysis (TGA) curves of the PMMA-*g*-$BaTiO_3$, BT-APTMS-Br, and bare $BaTiO_3$ nanoparticles.

The films of PMMA-*g*-$BaTiO_3$ including PB42, PB37, and PB24 were cast from toluene and tested for dielectric properties. To decouple the effects of polymer grafting, solutions of bare $BaTiO_3$ nanoparticles and PMMA (mol mass 106 000 g/mol) were prepared and are termed "blends" here. The ratios of bare particles with respect to PMMA in blends were maintained at 42%, 37%, and 24% to accurately mimic the PGNP concentrations. Figure 3A shows the dielectric permittivity (ε_r) of the PGNP as well as the blend samples. In general, the permittivity increases with an increasing amount of $BaTiO_3$ nanoparticles for both PGNPs and bare nanoparticle−polymer blends. The permittivities of the PGNP samples and the blend samples are comparable to each other, showing that the polymer grafting does not significantly affect the nanoparticle polarizability under an electric field. Furthermore, these permittivities are comparable with those observed for the $BaTiO_3$ PMMA PGNPs studied in the literature[30,37] for the same nanoparticle concentration. For the PGNPs and blends studied here, PB42 shows the highest permittivity of 9.89 ± 3 at a frequency of 1 kHz.

Figure 3B shows the loss tangent (tan δ) of the PGNP and blend samples as a function of frequency. The loss tangent for the blends as well as PGNPs is lower than 0.1 in the frequency range of 1 kHz to 1 MHz. Additionally, the loss tangent of PGNPs with higher nanoparticle fractions, i.e., PB42 and PB37, is less than their blend counterparts, which might be due to the low graft density of the PB42 and PB37 PGNPs. The lower graft density enables the "star-polymer"-like behavior of PGNPs by enabling polymer entanglement.[63] This in turn might decrease the loss tangent of the PGNPs. Higher graft density, on the other hand, causes the PGNPs to behave like hard spheres, which might increase the loss tangent of the

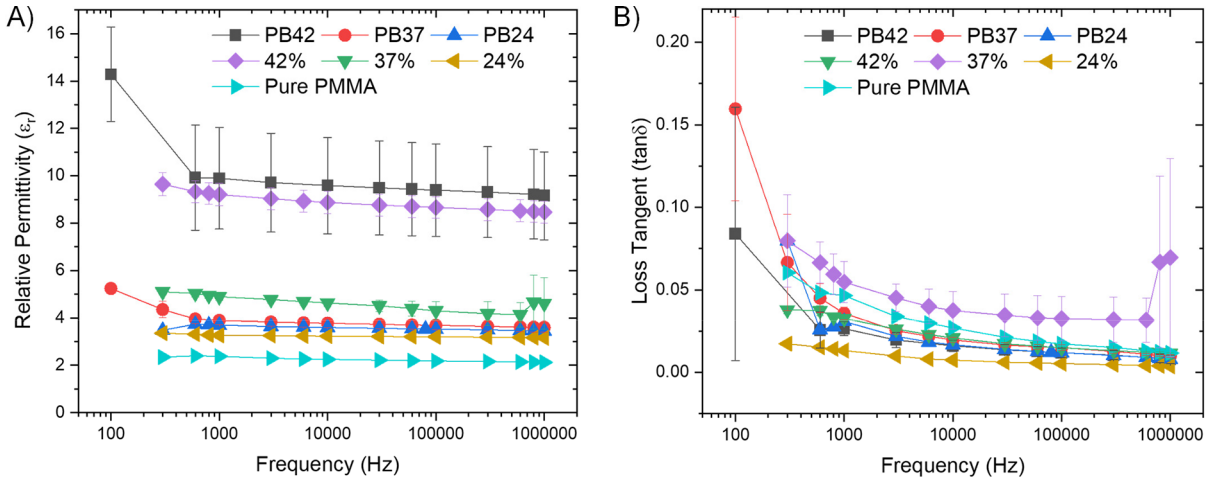

Figure 3. (A) Dielectric permittivity (ε_r) and (B) loss tangent (tan δ) of $BaTiO_3$ grafted PMMA PGNPs PB42, PB37, and PB24, where 42, 37, and 24 denote the mass % fraction of nanoparticles in single-component PGNPs, blends of PMMA with bare nanoparticles in the weight fraction of 42 mass %, 37 mass %, and 24 mass %, and pure PMMA. The permittivity increases with increasing the fraction of the nanoparticles in PGNPs as well as blends, with PGNP permittivities being comparable to the blend permittivities. Low grafting density PGNPs i.e., PB42 and PB37, show lower loss tangent as compared to their blend counterparts due to polymer interpenetration and "star-polymer"-like nature.

https://doi.org/10.1021/jacsau.3c00022
JACS Au 2023, 3, 1365−1375

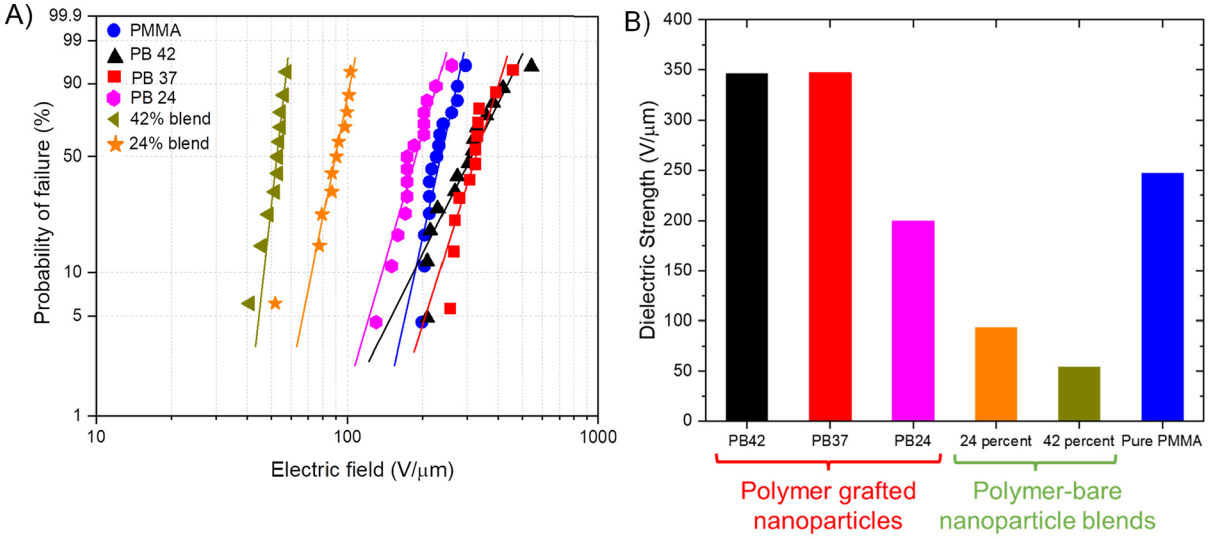

Figure 4. (A) Weibull probability plots and (B) Weibull dielectric strength, which shows an electric field at 63.2% probability of failure for $BaTiO_3$-grafted PMMA PGNPs PB42, PB37, and PB24, where 42, 37, and 24 denote the mass % fraction of nanoparticles in single-component PGNPs, blends of PMMA with bare nanoparticles in the weight fraction of 42 mass % and 24 mass %, and pure PMMA. The dielectric strength of PGNPs is significantly higher than their blends' counterparts, which might be due to the uniform distribution of particles in the polymer matrices and reduced dielectric contrast between the polymer and the nanoparticles.

PGNPs. Here, we observe that the high graft density PB24 PGNP exhibits a higher loss tangent compared to its blend counterpart.

In addition to the dielectric permittivity of the dielectric materials, the dielectric strength is another important property that dictates the capacitive energy storage properties of the dielectric capacitors. Given that the dielectric strength is the measure of a material's ability to withstand an electric field, it dictates the maximum energy that the material can store without undergoing failure. In the context of polymeric nanocomposites, the dielectric strength is dictated by the dielectric strength of the polymer, nanofillers, and the interactions of polymer and nanofillers. Usually, with adding inorganic nanofillers such as $BaTiO_3$ in polymers, the dielectric strength decreases significantly[1] due to particle aggregation, and increased electrical stress at the particle−polymer interface. We expect that the particle grafting to the nanoparticles can alleviate these problems given that the polymer grafting enables uniform particle distribution and can decrease electrical stresses at the interface due to the covalent bonding between the particle and polymer.

The dielectric strengths of the polymer grafted nanoparticles, polymer−bare nanoparticle blends, and pure PMMA are analyzed using the two-parameter Weibull equation given by

$$P(E) = 1 - \exp\left(-\left(\frac{E}{E_{BD}}\right)^{\beta}\right) \quad (2)$$

where $P(E)$ is the cumulative probability of dielectric failure, E is the measured dielectric strength, E_{BD} is the Weibull dielectric strength, i.e., the dielectric strength at 63.2% probability of failure, and β is the fitting parameter. Figure 4A shows the Weibull probability plots of the polymer-grafted nanoparticles PB42, PB37, and PB24 compared to the polymer and bare nanoparticle blends with 42% and 24% nanoparticle loadings and pure PMMA. It is evident from the plots that the blends have a higher probability of failure at lower electric fields, while the probability of failure of PGNPs is comparable to that of the pure polymer.

Figure 4B shows the Weibull dielectric strengths calculated at 63.2% probability of failure. The Weibull dielectric strengths of PB42, PB37, PB24, 42% blend, 24% blend, and pure PMMA are 346 V/μm (β = 3.55), 347 V/μm (β = 5.65), 199.7 V/μm (β = 6.07), 53.75 V/μm (β = 15.76), 93.45 V/μm (β = 8.83), and 246.95 V/μm (β = 8.04), respectively. The polymer-grafted nanoparticles show significantly higher dielectric strength than their blend counterparts. This significant increment might be due to the highly uniform distribution of nanoparticles and reduced electric field stress at the polymer−particle interface in grafted nanoparticle-based composites. Furthermore, given that the nanoparticle fractions are high in PGNPs and blends (24% to 42%), these effects might be amplified further. As expected, the dielectric strengths of bare nanoparticle−polymers blends are higher at lower nanoparticles loadings of 2 and 5 mass % (Figure S9), although the permittivities are also lower at these mass fractions (Figure S8).

It is interesting to note that while PB24 has lower $BaTiO_3$ content, its dielectric strength is still lower than the higher $BaTiO_3$ content PB42 and PB37 PGNP nanocomposites. The grafting density of PB24 is around 0.929 chains/nm^2, which is much higher than the grafting densities of PB42 (0.303 chains/nm^2) and PB37 (0.470 chains/nm^2). The higher grafting density of the PGNPs caused the nanoparticles to behave like "hard-sphere"-like particles,[63] which have minimum polymer interpenetration and entanglements. Furthermore, these have high chain-end densities known to enhance breakdown. Together, these reduce the electrical stress dissipation and trigger the dielectric breakdown of the nanocomposites. The low-grafted density PGNPs PB42 and PB37, on the other hand, have a higher dielectric strength due to their lower chain-end density and "star-polymer"-like behavior.[63] This shows that the dielectric strength of PGNPs is dictated by a combination of multiple factors including graft density,

https://doi.org/10.1021/jacsau.3c00022
JACS Au 2023, 3, 1365−1375

nanoparticle fraction, grafted polymer, the type of nanoparticle, and polymer molecular weight.

The maximum energy stored inside a dielectric material can be calculated using the material's permittivity and dielectric strength by

$$U_{max} = \frac{1}{2}\varepsilon_0\varepsilon_r {E_{BD}}^2 \quad (3)$$

where ε_0 is the permittivity of free space, ε_r is relative permittivity, E_{BD} is the dielectric strength, and U_{max} is the maximum energy stored in the dielectric material. The maximum energy densities of the polymer grafted nanoparticles, blends, and pure PMMA as calculated from eq 2 are plotted in Figure 5 and mentioned in Table 2 with the rest of

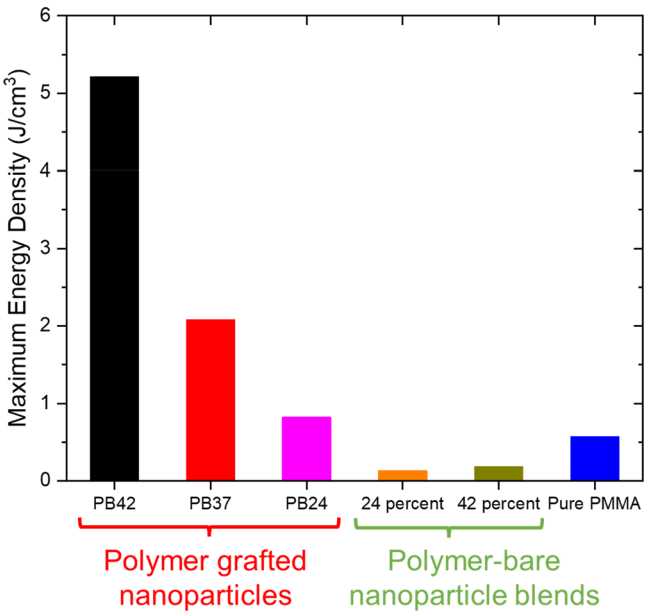

Figure 5. Comparison of the maximum energy density of $BaTiO_3$ PGNPs, bare $BaTiO_3$ and PMMA blends, and pure PMMA films. The PGNPs display the potential of higher energy density as compared to their blend counterparts due to uniform particle distribution and reduced electrical stress on the particles, with PB42 having 42% $BaTiO_3$ content and low grafting density of 0.3 chains/nm^2 reaching a maximum energy density of ≈5.2 J/cm^3.

the PGNP and blends parameters. The polymer-grafted nanoparticles demonstrate higher energy density as compared to their blend counterparts on account of higher dielectric strength. Furthermore, PB42, which has the highest nanoparticle content (≈42%) and lowest grafting density (≈0.303 chains/nm^2), shows the highest energy density of ≈5.2 J/cm^3, which is significantly higher than those of commercial dielectric capacitors (≈(1 to 2) J/cm^3).

The polymer-grafted nanoparticles' capability to store high energy density due to the grafted polymer chains is highly facile and versatile, especially as it does not need developing any new materials. Furthermore, the tunability of dielectric properties by simply tuning grafting density and polymer molecular weight demonstrates the versatility of polymer-grafted nanoparticles for developing materials with tailored properties and shows the fine interplay between the structure–property relationship of these materials as well as between the polymer physics and the energy storage capabilities of polymeric nanocomposites.

CONCLUSIONS

In conclusion, core–shell structured PMMA-*g*-$BaTiO_3$ NPs with varying molecular mass and graft density were synthesized via the "grafting from" approach by performing hydroxylation (H_2O_2) followed by silylation (APTMS), anchoring of ATRP initiator (BIB) agent, and the final step of SI-ATRP polymerizations of MMA on $BaTiO_3$ nanoparticles. The FTIR and ^{1}H NMR measurements established successful grafting of PMMA on nanoparticles. GPC measurements of polymer cleaved from PGNPs exhibited molecular mass ((97700 to130000) g/mol) with lower polydispersity, and the molecular mass of the grafted chain was influenced by the feed ratio. TEM confirmed successful grafting of $BaTiO_3$ NPs with PMMA with shell thickness in the range of (3 to 10) nm, and the shell thickness was tunable based on the feed ratio. The evaluation of the dielectric performance of hybrid core–shell single-component nanocomposites showed variable dielectric constant ε_r (3.7 to 9.9) and low dielectric loss (<0.05) with high breakdown strength ((200 to 347) V/μm), resulting in energy densities ranging from 0.82 J/cm^3 to 5.2 J/cm^3. In particular, the grafted nanoparticles with the highest molecular weight and lowest grafting density showed an energy density of ≈5.2 J/cm^3, which is an order of magnitude higher than their blend counterparts. Furthermore, the tunability of dielectric and energy storage properties by varying polymer grafting density and nanoparticle loading provides unparalleled control over the material properties of these nanocomposites.

ASSOCIATED CONTENT

Supporting Information

The Supporting Information is available free of charge at https://pubs.acs.org/doi/10.1021/jacsau.3c00022.

FTIR spectra for PGNPs, NMR spectra, and GPC traces for cleaved polymers, DLS results, and dielectric properties at low particle loading (PDF)

Table 2. Results of the Dielectric Performance of $BaTiO_3$-*g*-PMMA

polymer nanocomposite	permittivity	breakdown voltage, E_{BD} (V/μm)	energy density, U (J/cm^3)	char yield (%)	mol mass, M_w	grafting density (chains/nm^2)
PB42 (PGNP)	9.89 ± 3	346.2	5.21	41.7	130000	0.303
PB37 (PGNP)	3.9 ± 0.2	347.1	2.08	37.3	97000	0.470
PB24 (PGNP)	3.7 ± 0.2	199.7	0.82	24.08	100080	0.929
PMMA + 24% BT (blend)	3.26	93.45	0.13		106000	
PMMA + 42% BT (blend)	9.21 ± 0.4	53.75	0.18		106000	
pure PMMA	2.11 ± 0.4	246.9	0.57		106 000	

https://doi.org/10.1021/jacsau.3c00022
JACS Au 2023, 3, 1365–1375

AUTHOR INFORMATION

Corresponding Authors

Bhausaheb V. Tawade − *Department of Chemistry, Howard University, Washington, D.C. 20059, United States;* orcid.org/0000-0001-7385-3643; Email: bvtawade@gmail.com

Maninderjeet Singh − *Department of Chemical and Biomolecular Engineering, University of Houston, Houston, Texas 77204, United States;* orcid.org/0000-0001-8891-8454; Email: msingh9@central.uh.edu

Alamgir Karim − *Department of Chemical and Biomolecular Engineering, University of Houston, Houston, Texas 77204, United States;* orcid.org/0000-0003-1302-9374; Email: akarim3@central.uh.edu

Dharmaraj Raghavan − *Department of Chemistry, Howard University, Washington, D.C. 20059, United States;* orcid.org/0000-0002-7634-0656; Email: draghavan@howard.edu

Authors

Ikeoluwa E. Apata − *Department of Chemistry, Howard University, Washington, D.C. 20059, United States;* orcid.org/0000-0003-2508-3255

Jagadesh Veerasamy − *Department of Chemical and Biomolecular Engineering, University of Houston, Houston, Texas 77204, United States*

Nihar Pradhan − *Department of Chemistry, Physics and Atmospheric Science, Jackson State University, Jackson, Mississippi 39217, United States;* orcid.org/0000-0002-3912-4233

Jack F. Douglas − *Material Science and Engineering Division, National Institute of Standards and Technology, Gaithersburg, Maryland 20899, United States;* orcid.org/0000-0001-7290-2300

Complete contact information is available at: https://pubs.acs.org/10.1021/jacsau.3c00022

Author Contributions

⊥B.V.T. and M.S. made equal contributions to this work. CRediT: **Bhausaheb V Tawade** conceptualization, data curation, formal analysis, investigation, methodology, writing-original draft, writing-review & editing; **Maninderjeet Singh** conceptualization, data curation, formal analysis, investigation, methodology, writing-original draft, writing-review & editing; **Ikeoluwa Apata** conceptualization, data curation, formal analysis, investigation, methodology, writing-review & editing; **Jagadesh Veerasamy** data curation, methodology; **Nihar Ranjan Pradhan** formal analysis, funding acquisition; **Alamgir Karim** conceptualization, formal analysis, project administration, supervision, writing-review & editing; **Jack F. Douglas** formal analysis, writing-review & editing; **Dharmaraj Raghavan** conceptualization, formal analysis, funding acquisition, project administration, writing-review & editing.

Notes

The authors declare no competing financial interest.

Disclaimer: Certain commercial equipment, instruments, or materials are identified in this paper to foster understanding. Such identification does not imply recommendation or endorsement by the National Institute of Standards and Technology, nor does it imply that the materials or equipment identified are necessarily the best available for the purpose.

ACKNOWLEDGMENTS

The project was supported by NSF Grant DMR1901127. The authors thank Dr. Nagarjuna Gavvalapalli and Mr. Manikandan Mohanan, Georgetown University, Washington, DC, for help in performing GPC analysis.

REFERENCES

(1) Singh, M.; Apata, I. E.; Samant, S.; Wu, W.; Tawade, B. V.; Pradhan, N.; Raghavan, D.; Karim, A. Nanoscale Strategies to Enhance the Energy Storage Capacity of Polymeric Dielectric Capacitors: Review of Recent Advances. *Polym. Rev.* **2022**, *62*, 211−260.

(2) Baer, E.; Zhu, L. 50th Anniversary Perspective: Dielectric Phenomena in Polymers and Multilayered Dielectric Films. *Macromolecules* **2017**, *50* (6), 2239−2256.

(3) Nelson, J. K. *Dielectric Polymer Nanocomposites*; Springer: Boston, MA, 2010.

(4) Huan, T. D.; Boggs, S.; Teyssedre, G.; Laurent, C.; Cakmak, M.; Kumar, S.; Ramprasad, R. Advanced Polymeric Dielectrics for High Energy Density Applications. *Prog. Mater. Sci.* **2016**, *83*, 236−269.

(5) Tawade, B. V.; Apata, I. E.; Singh, M.; Das, P.; Pradhan, N.; Al-Enizi, A. M.; Karim, A.; Raghavan, D. Recent Developments in the Synthesis of Chemically Modified Nanomaterials for Use in Dielectric and Electronics Applications. *Nanotechnology* **2021**, *32* (14), 142004.

(6) Tawade, B. V.; Apata, I. E.; Pradhan, N.; Karim, A.; Raghavan, D. Recent Advances in the Synthesis of Polymer-Grafted Low-K and High-K Nanoparticles for Dielectric and Electronic Applications. *Molecules* **2021**, *26* (10), 2942.

(7) Samant, S. P.; Grabowski, C. A.; Kisslinger, K.; Yager, K. G.; Yuan, G.; Satija, S. K.; Durstock, M. F.; Raghavan, D.; Karim, A. Directed Self-Assembly of Block Copolymers for High Breakdown Strength Polymer Film Capacitors. *ACS Appl. Mater. Interfaces* **2016**, *8* (12), 7966−7976.

(8) Samant, S.; Basutkar, M.; Singh, M.; Masud, A.; Grabowski, C. A.; Kisslinger, K.; Strzalka, J.; Yuan, G.; Satija, S.; Apata, I.; Raghavan, D.; Durstock, M.; Karim, A. Effect of Molecular Weight and Layer Thickness on the Dielectric Breakdown Strength of Neat and Homopolymer Swollen Lamellar Block Copolymer Films. *ACS Appl. Polym. Mater.* **2020**, *2* (8), 3072−3083.

(9) Hailu, S. T.; Samant, S.; Grabowski, C.; Durstock, M.; Karim, A.; Raghavan, D. Synthesis of Highly Dispersed, Block Copolymer-Grafted TiO 2 Nanoparticles within Neat Block Copolymer Films. *J. Polym. Sci. Part A Polym. Chem.* **2015**, *53* (3), 468−478.

(10) Singh, M.; Dong, M.; Wu, W.; Nejat, R.; Tran, D. K.; Pradhan, N.; Raghavan, D.; Douglas, J. F.; Wooley, K. L.; Karim, A. Enhanced Dielectric Strength and Capacitive Energy Density of Cyclic Polystyrene Films. *ACS Polym. Au* **2022**, *5*, 324−332.

(11) Grabowski, C. A.; Koerner, H.; Meth, J. S.; Dang, A.; Hui, C. M.; Matyjaszewski, K.; Bockstaller, M. R.; Durstock, M. F.; Vaia, R. A. Performance of Dielectric Nanocomposites: Matrix-Free, Hairy Nanoparticle Assemblies and Amorphous Polymer−Nanoparticle Blends. *ACS Appl. Mater. Interfaces* **2014**, *6* (23), 21500−21509.

(12) Yan, J.; Bockstaller, M. R.; Matyjaszewski, K. Brush-Modified Materials: Control of Molecular Architecture, Assembly Behavior, Properties and Applications. *Prog. Polym. Sci.* **2020**, *100*, No. 101180.

(13) Hui, C. M.; Pietrasik, J.; Schmitt, M.; Mahoney, C.; Choi, J.; Bockstaller, M. R.; Matyjaszewski, K. Surface-Initiated Polymerization as an Enabling Tool for Multifunctional (Nano-)Engineered Hybrid Materials. *Chem. Mater.* **2014**, *26*, 745−762.

(14) Bicerano, J.; Douglas, J. F.; Brune, D. A. Model for the Viscosity of Particle Dispersions. *J. Macromol. Sci. Part C Polym. Rev.* **1999**, *39* (4), 561−642.

(15) Chremos, A.; Douglas, J. F. Communication: When Does a Branched Polymer Become a Particle? *J. Chem. Phys.* **2015**, *143* (11), 111104.

(16) Chremos, A.; Douglas, J. F. A Comparative Study of Thermodynamic, Conformational, and Structural Properties of

Bottlebrush with Star and Ring Polymer Melts. *J. Chem. Phys.* **2018**, *149* (4), No. 044904.
(17) Chremos, A.; Douglas, J. F. Hidden Hyperuniformity in Soft Polymeric Materials. *Phys. Rev. Lett.* **2018**, *121* (25), No. 258002.
(18) Chremos, A.; Douglas, J. F. Particle Localization and Hyperuniformity of Polymer-grafted Nanoparticle Materials. *Ann. Phys.* **2017**, *529* (5), 1600342.
(19) Chremos, A. Design of Nearly Perfect Hyperuniform Polymeric Materials. *J. Chem. Phys.* **2020**, *153* (5), No. 054902.
(20) Torquato, S. Hyperuniform States of Matter. *Phys. Rep.* **2018**, *745*, 1−95.
(21) Srivastava, S.; Agarwal, P.; Mangal, R.; Koch, D. L.; Narayanan, S.; Archer, L. A. Hyperdiffusive Dynamics in Newtonian Nanoparticle Fluids. *ACS Macro Lett.* **2015**, *4* (10), 1149−1153.
(22) Chremos, A.; Douglas, J. F. Influence of Branching on the Configurational and Dynamical Properties of Entangled Polymer Melts. *Polymers (Basel).* **2019**, *11* (6), 1045.
(23) Bhadauriya, S.; Wang, X.; Pitliya, P.; Zhang, J.; Raghavan, D.; Bockstaller, M. R.; Stafford, C. M.; Douglas, J. F.; Karim, A. Tuning the Relaxation of Nanopatterned Polymer Films with Polymer-Grafted Nanoparticles: Observation of Entropy−Enthalpy Compensation. *Nano Lett.* **2018**, *18* (12), 7441−7447.
(24) Bhadauriya, S.; Wang, X.; Nallapaneni, A.; Masud, A.; Wang, Z.; Lee, J.; Bockstaller, M. R.; Al-Enizi, A. M.; Camp, C. H., Jr.; Stafford, C. M.; Douglas, J. F.; Karim, A. Observation of General Entropy−Enthalpy Compensation Effect in the Relaxation of Wrinkled Polymer Nanocomposite Films. *Nano Lett.* **2021**, *21* (3), 1274−1281.
(25) Bilchak, C. R.; Jhalaria, M.; Huang, Y.; Abbas, Z.; Midya, J.; Benedetti, F. M.; Parisi, D.; Egger, W.; Dickmann, M.; Minelli, M.; Doghieri, F.; Nikoubashman, A.; Durning, C. J.; Vlassopoulos, D.; Jestin, J.; Smith, Z. P.; Benicewicz, B. C.; Rubinstein, M.; Leibler, L.; Kumar, S. K. Tuning Selectivities in Gas Separation Membranes Based on Polymer-Grafted Nanoparticles. *ACS Nano* **2020**, *14* (12), 17174−17183.
(26) Bilchak, C. R.; Huang, Y.; Benicewicz, B. C.; Durning, C. J.; Kumar, S. K. High-Frequency Mechanical Behavior of Pure Polymer-Grafted Nanoparticle Constructs. *ACS Macro Lett.* **2019**, *8* (3), 294−298.
(27) Choi, J.; Hui, C. M.; Pietrasik, J.; Dong, H.; Matyjaszewski, K.; Bockstaller, M. R. Toughening Fragile Matter: Mechanical Properties of Particle Solids Assembled from Polymer-Grafted Hybrid Particles Synthesized by ATRP. *Soft Matter* **2012**, *8* (15), 4072.
(28) Samant, S.; Hailu, S. T.; Al-Enizi, A. M.; Karim, A.; Raghavan, D. Orientation Control in Nanoparticle Filled Block Copolymer Cold Zone Annealed Films. *J. Polym. Sci., Part B: Polym. Phys.* **2015**, *53* (8), 604−614.
(29) Xie, L.; Huang, X.; Yang, K.; Li, S.; Jiang, P. Grafting to" Route to PVDF-HFP-GMA/BaTiO3 Nanocomposites with High Dielectric Constant and High Thermal Conductivity for Energy Storage and Thermal Management Applications. *J. Mater. Chem. A* **2014**, *2* (15), 5244.
(30) Yang, K.; Huang, X.; Zhu, M.; Xie, L.; Tanaka, T.; Jiang, P. Combining RAFT Polymerization and Thiol−Ene Click Reaction for Core−Shell Structured Polymer@BaTiO 3 Nanodielectrics with High Dielectric Constant, Low Dielectric Loss, and High Energy Storage Capability. *ACS Appl. Mater. Interfaces* **2014**, *6* (3), 1812−1822.
(31) Ma, J.; Azhar, U.; Zong, C.; Zhang, Y.; Xu, A.; Zhai, C.; Zhang, L.; Zhang, S. Core-Shell Structured PVDF@BT Nanoparticles for Dielectric Materials: A Novel Composite to Prove the Dependence of Dielectric Properties on Ferroelectric Shell. *Mater. Des.* **2019**, *164*, No. 107556.
(32) Jiang, B.; Pang, X.; Li, B.; Lin, Z. Organic-Inorganic Nanocomposites via Placing Monodisperse Ferroelectric Nanocrystals in Direct and Permanent Contact with Ferroelectric Polymers. *J. Am. Chem. Soc.* **2015**, *137* (36), 11760−11767.
(33) Pang, X.; He, Y.; Jiang, B.; Iocozzia, J.; Zhao, L.; Guo, H.; Liu, J.; Akinc, M.; Bowler, N.; Tan, X.; Lin, Z. Block Copolymer/Ferroelectric Nanoparticle Nanocomposites. *Nanoscale* **2013**, *5* (18), 8695.
(34) Pang, X.; Zhao, L.; Akinc, M.; Kim, J. K.; Lin, Z. Novel Amphiphilic Multi-Arm, Star-Like Block Copolymers as Unimolecular Micelles. *Macromolecules* **2011**, *44* (10), 3746−3752.
(35) Guo, H. Z.; Mudryk, Y.; Ahmad, M. I.; Pang, X. C.; Zhao, L.; Akinc, M.; Pecharsky, V. K.; Bowler, N.; Lin, Z. Q.; Tan, X. Structure Evolution and Dielectric Behavior of Polystyrene-Capped Barium Titanate Nanoparticles. *J. Mater. Chem.* **2012**, *22*, 23944−23951.
(36) Wang, J.-S.; Matyjaszewski, K. Controlled/"living" Radical Polymerization. Atom Transfer Radical Polymerization in the Presence of Transition-Metal Complexes. *J. Am. Chem. Soc.* **1995**, *117* (20), 5614−5615.
(37) Xie, L.; Huang, X.; Wu, C.; Jiang, P. Core-Shell Structured Poly(Methyl Methacrylate)/BaTiO3 Nanocomposites Prepared by in Situ Atom Transfer Radical Polymerization: A Route to High Dielectric Constant Materials with the Inherent Low Loss of the Base Polymer. *J. Mater. Chem.* **2011**, *21* (16), 5897.
(38) Paniagua, S. A.; Kim, Y.; Henry, K.; Kumar, R.; Perry, J. W.; Marder, S. R. Surface-Initiated Polymerization from Barium Titanate Nanoparticles for Hybrid Dielectric Capacitors. *ACS Appl. Mater. Interfaces* **2014**, *6* (5), 3477−3482.
(39) Zhang, X.; Zhao, S.; Wang, F.; Ma, Y.; Wang, L.; Chen, D.; Zhao, C.; Yang, W. Improving Dielectric Properties of BaTiO3/Poly(Vinylidene Fluoride) Composites by Employing Core-Shell Structured BaTiO3@Poly(Methylmethacrylate) and BaTiO3@Poly-(Trifluoroethyl Methacrylate) Nanoparticles. *Appl. Surf. Sci.* **2017**, *403*, 71−79.
(40) You, N.; Zhang, C.; Liang, Y.; Zhang, Q.; Fu, P.; Liu, M.; Zhao, Q.; Cui, Z.; Pang, X. Facile Fabrication of Size-Tunable Core/Shell Ferroelectric/Polymeric Nanoparticles with Tailorable Dielectric Properties via Organocatalyzed Atom Transfer Radical Polymerization Driven by Visible Light. *Sci. Rep.* **2019**, *9* (1), 1869.
(41) Wang, J.; Guan, F.; Cui, L.; Pan, J.; Wang, Q.; Zhu, L. Achieving High Electric Energy Storage in a Polymer Nanocomposite at Low Filling Ratios Using a Highly Polarizable Phthalocyanine Interphase. *J. Polym. Sci., Part B: Polym. Phys.* **2014**, *52* (24), 1669−1680.
(42) Bobnar, V.; Levstik, A.; Huang, C.; Zhang, Q. M. Intrinsic Dielectric Properties and Charge Transport in Oligomers of Organic Semiconductor Copper Phthalocyanine. *Phys. Rev. B* **2005**, *71* (4), No. 041202.
(43) Nalwa, H. S.; Dalton, L. R.; Vasudevan, P. Dielectric Properties of Copper-Phthalocyanine Polymer. *Eur. Polym. J.* **1985**, *21* (11), 943−947.
(44) Xie, L.; Huang, X.; Huang, Y.; Yang, K.; Jiang, P. Core@Double-Shell Structured BaTiO 3 − Polymer Nanocomposites with High Dielectric Constant and Low Dielectric Loss for Energy Storage Application. *J. Phys. Chem. C* **2013**, *117* (44), 22525−22537.
(45) Zhang, X.; Chen, H.; Ma, Y.; Zhao, C.; Yang, W. Preparation and Dielectric Properties of Core−Shell Structural Composites of Poly(1H,1H,2H,2H-Perfluorooctyl Methacrylate)@BaTiO3 Nanoparticles. *Appl. Surf. Sci.* **2013**, *277*, 121−127.
(46) Bouharras, F. E.; Raihane, M.; Silly, G.; Totee, C.; Ameduri, B. Core−Shell Structured Poly(Vinylidene Fluoride)- Grafted -BaTiO 3 Nanocomposites Prepared via Reversible Addition−Fragmentation Chain Transfer (RAFT) Polymerization of VDF for High Energy Storage Capacitors. *Polym. Chem.* **2019**, *10* (7), 891−904.
(47) Zhu, M.; Huang, X.; Yang, K.; Zhai, X.; Zhang, J.; He, J.; Jiang, P. Energy Storage in Ferroelectric Polymer Nanocomposites Filled with Core−Shell Structured Polymer@BaTiO 3 Nanoparticles: Understanding the Role of Polymer Shells in the Interfacial Regions. *ACS Appl. Mater. Interfaces* **2014**, *6* (22), 19644−19654.
(48) Qian, K.; Lv, X.; Chen, S.; Luo, H.; Zhang, D. Interfacial Engineering Tailoring the Dielectric Behavior and Energy Density of BaTiO 3 /P(VDF-TrFE-CTFE) Nanocomposites by Regulating a Liquid-Crystalline Polymer Modifier Structure. *Dalt. Trans.* **2018**, *47* (36), 12759−12768.

https://doi.org/10.1021/jacsau.3c00022
JACS Au 2023, 3, 1365−1375

(49) Chen, S.; Lv, X.; Han, X.; Luo, H.; Bowen, C. R.; Zhang, D. Significantly Improved Energy Density of BaTiO 3 Nanocomposites by Accurate Interfacial Tailoring Using a Novel Rigid-Fluoro-Polymer. *Polym. Chem.* **2018**, *9* (5), 548−557.
(50) Cao, X. T.; Showkat, A. M.; Lee, W.-K.; Lim, K. T. Luminescence of Terbium (III) Complexes Incorporated in Carboxylic Acid Functionalized Polystyrene/BaTiO 3 Nanocomposites. *Mol. Cryst. Liq. Cryst.* **2015**, *622* (1), 36−43.
(51) Zhang, D.; Ma, C.; Zhou, X.; Chen, S.; Luo, H.; Bowen, C. R.; Zhou, K. High Performance Capacitors Using BaTiO 3 Nanowires Engineered by Rigid Liquid-Crystalline Polymers. *J. Phys. Chem. C* **2017**, *121* (37), 20075−20083.
(52) Qiao, Y.; Yin, X.; Wang, L.; Islam, M. S.; Benicewicz, B. C.; Ploehn, H. J.; Tang, C. Bimodal Polymer Brush Core−Shell Barium Titanate Nanoparticles: A Strategy for High-Permittivity Polymer Nanocomposites. *Macromolecules* **2015**, *48* (24), 8998−9006.
(53) Qiao, Y.; Islam, M. S.; Han, K.; Leonhardt, E.; Zhang, J.; Wang, Q.; Ploehn, H. J.; Tang, C. Polymers Containing Highly Polarizable Conjugated Side Chains as High-Performance All-Organic Nanodielectric Materials. *Adv. Funct. Mater.* **2013**, *23* (45), 5638−5646.
(54) Qiao, Y.; Islam, M. S.; Wang, L.; Yan, Y.; Zhang, J.; Benicewicz, B. C.; Ploehn, H. J.; Tang, C. Thiophene Polymer-Grafted Barium Titanate Nanoparticles toward Nanodielectric Composites. *Chem. Mater.* **2014**, *26* (18), 5319−5326.
(55) Yang, K.; Huang, X.; Xie, L.; Wu, C.; Jiang, P.; Tanaka, T. Core-Shell Structured Polystyrene/BaTiO 3 Hybrid Nanodielectrics Prepared by In Situ RAFT Polymerization: A Route to High Dielectric Constant and Low Loss Materials with Weak Frequency Dependence. *Macromol. Rapid Commun.* **2012**, *33* (22), 1921−1926.
(56) Yang, K.; Huang, X.; Huang, Y.; Xie, L.; Jiang, P. Fluoro-Polymer@BaTiO 3 Hybrid Nanoparticles Prepared via RAFT Polymerization: Toward Ferroelectric Polymer Nanocomposites with High Dielectric Constant and Low Dielectric Loss for Energy Storage Application. *Chem. Mater.* **2013**, *25* (11), 2327−2338.
(57) Lettow, J. H.; Yang, H.; Nealey, P. F.; Rowan, S. J. Effect of Graft Molecular Weight and Density on the Mechanical Properties of Polystyrene-Grafted Cellulose Nanocrystal Films. *Macromolecules* **2021**, *54* (22), 10594−10604.
(58) Lettow, J. H.; Kaplan, R. Y.; Nealey, P. F.; Rowan, S. J. Enhanced Ion Conductivity through Hydrated, Polyelectrolyte-Grafted Cellulose Nanocrystal Films. *Macromolecules* **2021**, *54* (14), 6925−6936.
(59) Santos, P. J.; Gabrys, P. A.; Zornberg, L. Z.; Lee, M. S.; Macfarlane, R. J. Macroscopic Materials Assembled from Nanoparticle Superlattices. *Nature* **2021**, *591* (7851), 586−591.
(60) Benoit, D. N.; Zhu, H.; Lilierose, M. H.; Verm, R. A.; Ali, N.; Morrison, A. N.; Fortner, J. D.; Avendano, C.; Colvin, V. L. Measuring the Grafting Density of Nanoparticles in Solution by Analytical Ultracentrifugation and Total Organic Carbon Analysis. *Anal. Chem.* **2012**, *84* (21), 9238−9245.
(61) Chang, S.-J.; Liao, W.-S.; Ciou, C.-J.; Lee, J.-T.; Li, C.-C. An Efficient Approach to Derive Hydroxyl Groups on the Surface of Barium Titanate Nanoparticles to Improve Its Chemical Modification Ability. *J. Colloid Interface Sci.* **2009**, *329* (2), 300−305.
(62) Wang, Z.; Yan, J.; Liu, T.; Wei, Q.; Li, S.; Olszewski, M.; Wu, J.; Sobieski, J.; Fantin, M.; Bockstaller, M. R.; Matyjaszewski, K. Control of Dispersity and Grafting Density of Particle Brushes by Variation of ATRP Catalyst Concentration. *ACS Macro Lett.* **2019**, *8* (7), 859−864.
(63) Wu, W.; Singh, M.; Masud, A.; Wang, X.; Nallapaneni, A.; Xiao, Z.; Zhai, Y.; Wang, Z.; Terlier, T.; Bleuel, M.; Yuan, G.; Satija, S. K.; Douglas, J. F.; Matyjaszewski, K.; Bockstaller, M. R.; Karim, A. Control of Phase Morphology of Binary Polymer Grafted Nanoparticle Blend Films via Direct Immersion Annealing. *ACS Nano* **2021**, *15* (7), 12042−12056.

https://doi.org/10.1021/jacsau.3c00022
JACS Au 2023, 3, 1365−1375